Combination of host immune metabolic biomarkers for the PD-1 blockade cancer immunotherapy

Ryusuke Hatae,[1] Kenji Chamoto,[1] Young Hak Kim,[2] Kazuhiro Sonomura,[3,4] Kei Taneishi,[5,6] Shuji Kawaguchi,[3] Hironori Yoshida,[2] Hiroaki Ozasa,[2] Yuichi Sakamori,[2] Maryam Akrami,[1] Sidonia Fagarasan,[7] Izuru Masuda,[8] Yasushi Okuno,[5] Fumihiko Matsuda,[3] Toyohiro Hirai,[2] and Tasuku Honjo[1]

[1]Department of Immunology and Genomic Medicine, [2]Department of Respiratory Medicine, and [3]Center for Genomic Medicine, Graduate School of Medicine, Kyoto University, Kyoto, Japan. [4]Life Science Research Center, Technology Research Laboratory, Shimadzu Corporation, Kyoto, Japan. [5]Department of Biomedical Data Intelligence, Graduate School of Medicine, Kyoto University, Kyoto, Japan. [6]RIKEN Cluster for Science, Technology and Innovation Hub, Kobe, Japan. [7]Laboratory for Mucosal Immunity, Center for Integrative Medical Sciences, RIKEN Yokohama Institute, Yokohama, Japan. [8]Medical Examination Center, Takeda Hospital, Kyoto, Japan.

BACKGROUND. Current clinical biomarkers for the programmed cell death 1 (PD-1) blockade therapy are insufficient because they rely only on the tumor properties, such as programmed cell death ligand 1 expression frequency and tumor mutation burden. Identifying reliable, responsive biomarkers based on the host immunity is necessary to improve the predictive values.

METHODS. We investigated levels of plasma metabolites and T cell properties, including energy metabolism markers, in the blood of patients with non-small cell lung cancer before and after treatment with nivolumab ($n = 55$). Predictive values of combination markers statistically selected were evaluated by cross-validation and linear discriminant analysis on discovery and validation cohorts, respectively. Correlation between plasma metabolites and T cell markers was investigated.

RESULTS. The 4 metabolites derived from the microbiome (hippuric acid), fatty acid oxidation (butyrylcarnitine), and redox (cystine and glutathione disulfide) provided high response probability (AUC = 0.91). Similarly, a combination of 4 T cell markers, those related to mitochondrial activation (PPARγ coactivator 1 expression and ROS), and the frequencies of CD8+PD-1hi and CD4+ T cells demonstrated even higher prediction value (AUC = 0.96). Among the pool of selected markers, the 4 T cell markers were exclusively selected as the highest predictive combination, probably because of their linkage to the abovementioned metabolite markers. In a prospective validation set ($n = 24$), these 4 cellular markers showed a high accuracy rate for clinical responses of patients (AUC = 0.92).

CONCLUSION. Combination of biomarkers reflecting host immune activity is quite valuable for responder prediction.

FUNDING. AMED under grant numbers 18cm0106302h0003, 18gm0710012h0105, and 18lk1403006h0002; the Tang Prize Foundation; and JSPS KAKENHI grant numbers JP16H06149, 17K19593, and 19K17673.

Introduction

Programmed cell death 1 (PD-1) and cytotoxic T lymphocyte–associated protein 4 (CTLA-4) are the critical players in maintaining immune tolerance during tumor growth (1–4). Blocking of molecules individually or both together rejuvenates CD8+ T cells in the dormant or reversible exhaustion stage and can induce strong antitumor activity in mice and humans (1–3, 5, 6). CD8+ T cells, once activated by recognition of tumor antigens, proliferate and attack tumors. Activated T cells with chronic stimulation eventually express PD-1 and CTLA-4 and go into the reversible exhaustion stage to avoid excessive proliferation and the generation of autoimmunity. Some of the activated CD8+ T cells may go into the

irreversible exhaustion stage, resist rejuvenation, and are defined by PD-1^{hi}, CTLA-4^{hi}, T cell immuno-globulin and mucin domain–containing molecule 3–positive (Tim-3^{+}), Ki-67^{+}, and others (7). Immune tolerant individuals who carry tumors are likely to contain variable proportions of CD8^{+} T cells with reversible and irreversible exhaustion stages.

Although antibodies against CTLA-4, PD-1, or its ligand, PD-L1, have been approved for treatment of various human cancers and demonstrated the impressive clinical efficacy (4), a significant portion of cancer patients remain less responsive (4–6). Therefore, predictive biomarkers to distinguish responders and non-responders are desperately required to save cost and time for those patients.

Effective cancer immunotherapy depends on the cancer-immunity cycle, in which naive T cells are primed in draining lymph nodes (DLNs) and differentiated to effector T cells that egress into circulation and traffic to tumor sites, guided by a gradient of chemokines released from tumor sites to attack tumor cells (8). Tumor antigens are captured by dendritic cells, which in turn traffic to DLNs and stimulate naive T cells again. To distinguish responders from nonresponders, it is critical to evaluate how many CD8^{+} T cells are in the stage of reversible or irreversible exhaustion in patients by monitoring peripheral blood mononuclear cells (PBMCs), while the actual battles of the immune system against cancer take place in tumor sites and DLNs.

When CD8^{+} T cells are activated by antigenic stimulation, such as tumor antigens, they mobilize various intracellular signaling pathways to generate abundant energy and anabolic reaction substrates required for proliferation (9). Fagarasan's group previously showed that proliferation of the antigen-stimulated T cell population drastically changes the systemic metabolites in mouse blood (10). We also confirmed similar drastic change in serum metabolites due to the antitumor immune reactions in a PD-1 blockade cancer therapy model (11). Activated tumor-reactive CD8^{+} T cells were also shown to carry mitochondria with higher reactive oxygen species (ROS) detected by mitochondrial dye staining. ROS signaling links to the regulation of mTOR/AMPK phosphorylation, which subsequently activates the PPARγ coactivator 1α (PGC-1α) pathway. This feed-forward pathway for mitochondrial biogenesis enhances CD8^{+} T cell activation (11, 12). We further showed that PGC-1α/PPAR complex activation enhances the efficacy of the PD-1 blockade therapy by enhancing fatty acid oxidation (FAO) in CD8^{+} T cells, which leads to longevity of effector CD8^{+} T cells (13). Therefore, these T cell metabolism-associated markers may serve as predictive or early monitoring biomarkers in the PD-1 blockade therapy.

It is also known that gut microbiota and immune activity mutually affect each other as Fagarasan and coworkers have demonstrated using IgA-deficient or PD-1–deficient mouse models (14, 15). In the case of tumor immunity, recent reports also suggested that microbiota and/or their metabolites are related to the efficacy of immune checkpoint inhibitors (16–18). Especially, certain microbiota, *Akkermansia muciniphila*, and diversity of flora are shown to correlate to the responsiveness to the PD-1 blockade therapy (18). However, it is still elusive whether any of the microbiota-associated factors could be responder biomarkers for the PD-1 blockade therapy.

Currently, PD-L1[hi] expression on histological tumor tissue samples is used as a responder predictive marker for non-small cell lung cancer (NSCLC) (19, 20). The FDA has recently approved micro-satellite instability–high or mismatch repair deficiency as common responder biomarkers for various solid tumors (21). These markers, however, cannot cover all the responsive patients, probably because the responses of tumor-reactive CD8^{+} T cells are affected not only by tumor properties but also by host immune activity (21). Several groups have identified candidates for responder biomarkers by analysis of various immune cell compartments at tumor sites or in peripheral blood. The proposed markers include the frequencies of CD8^{+} T cells, CD4^{+} T cells, eosinophils, neutrophils, subsets of suppressive macrophages, and subsets of T cells (16). Immune regulators, such as certain cytokines or chemokines, were also listed as candidates of biomarkers (16). However, the predictive value of each of these single markers for host immunity is not sufficient for clinical usage.

In the present studies using blood samples from 55 patients with NSCLC, we demonstrated that a combination of several plasma metabolites and/or T cell markers could serve as good responder biomarkers (AUC = 0.96 by cross-validation). The metabolite markers include those related to microbiota (hippuric acid), FAO (butyrylcarnitine), and redox (cystine and glutathione disulfide). The cellular markers of T cells in responders contain those associated with suppressive function (the PD-1^{hi} population) and mito-chondrial activities (PGC-1 and ROS expression) in CD8^{+} T cells. These T cell markers are linked with the metabolite markers described above. Therefore, we propose that the combinatorial quantitation of either

the specific plasma metabolites or PBMC T cell markers will be a highly predictive biomarker of the PD-1 blockade therapy for clinical usage.

Results

Microbiota metabolism– and energy metabolism–related metabolites correlate with responsiveness to the PD-1 blockade cancer immunotherapy. Accumulating evidence indicates there is a considerable association between immune responses and the metabolome (22). However, it remains unknown whether particular metabolites can serve as predictive biomarkers for the PD-1 blockade therapy in humans. In this study, we identified plasma metabolites and T cellular markers from 55 NSCLC patients (discovery cohort) and validated the markers in 24 patients (validation cohort) (Figure 1). To investigate how metabolites are associated with antitumor immunity first, we analyzed metabolites and T cell functional markers in plasma and PBMCs, respectively, in 55 patients with NSCLC before and after nivolumab treatment (Figure 2A and Supplemental Tables 1–4; supplemental material available online with this article; https://doi.org/10.1172/jci.insight.133501DS1). Blood was harvested just before the injection of nivolumab at 0, 2, and 4 weeks, and we designated these samples as the 1st, 2nd, and 3rd samples, respectively (Figure 2A). We defined responsive and unresponsive patients based on the criteria of progression-free survival (PFS) more than 3 months or PFS no more than 3 months according to the PFS data of phase III clinical studies of NSCLC patients where around 40% to 50% of patients died within 3 months (Supplemental Figure 1A and refs. 23, 24). Although PFS more than 6 months has often been used as a responder criterion, both criteria (PFS > 3 months and PFS > 6 months) provided similar overall survival (OS) curves in the present study (Supplemental Figure 1, B and C). Moreover, PD-L1 tumor proportion score (TPS) at tumor sites could not discriminate between responders and nonresponders clearly in the present study (Supplemental Figure 1, D and E). We measured 247 metabolites in 55 patients, of whom 8 had to stop the therapy because of severe side effects and other reasons, leaving us with the data of 47 patients for analysis (Figure 1 and Figure 2A). Volcano plot analysis of these metabolites based on fold change and P value demonstrated that hippuric acid in the 1st samples and hippuric acid, indoxyl sulfate, 4-cresol, and glutathione disulfide (GSSG) in the 3rd samples were significantly elevated in responders compared with nonresponders (Figure 2B and Table 1). On the other hand, the levels of α-ketoglutaric acid and butyrlcarnitine in the 3rd samples were lower in responders, but there were no items with significant differences between responders and nonresponders in the 2nd samples (Figure 2B and Table 1). Hippuric acid, indoxyl sulfate, and 4-cresol are reported to be almost exclusively produced by microbiota in mammals (25), which is consistent with the finding that patients treated with antibiotics within 3 months before the nivolumab treatment had lower levels of these 3 metabolites (Supplemental Figure 2A). Importantly, responsive patients had higher levels of the microbiota-derived metabolites (indoxyl sulfate and 4-cresol) than unresponsive patients, indicating that stronger antitumor immune responses are associated with the gut microenvironment (Figure 2C and Supplemental Figure 2B). We did not exclude those patients pretreated with antibiotics from this study because there were no differences in survival between patients treated with and without antibiotics at any time within 3 months before nivolumab injection (Supplemental Figure 2C). GSSG levels were higher in responders than in nonresponders, especially in the 3rd samples (Figure 2, B and D, and Table 1). GSSG is an oxidized form of glutathione, which controls the ROS levels appropriately in cells (26). Butyrylcarnitine levels were higher in nonresponders than in responders (Figure 2, B and D, and Table 1). Butyrylcarnitine, the 4-carbon acylcarnitine, serves as a fatty acid transporter into mitochondria to generate ATP. Acylcarnitine species with various amounts of carbon are released from cells once the function of FAO is attenuated (27–29). It should be noted that butyrylcarnitine and other acylcarnitine species (isovalerylcarnitine and hexanoylcarnitine) had a trend to increase in the later phase of therapy in nonresponders (Supplemental Figure 2D). There was a trend of lower α-ketoglutaric acid in responders than in nonresponders (Figure 2, B and D, and Table 1). In the tricarboxylic acid cycle in mitochondria for ATP production, α-ketoglutaric acid is a core metabolite and is reduced in the blood because of consumption by activated T cells (10, 11). Therefore, these data indicate that antitumor immune responses to the PD-1 blockade therapy are linked to microbiota and energy metabolism.

A combination of plasma metabolites can be a predictive biomarker. We addressed the probability of each predictive biomarker candidate selected above (Figure 2B and Table 1) by receiver operating characteristic (ROC) curve analysis with logistic regression. The AUC of each candidate was not high enough for prediction (right column in Table 1), though their AUCs were higher than that of PD-L1 TPS (0.66).
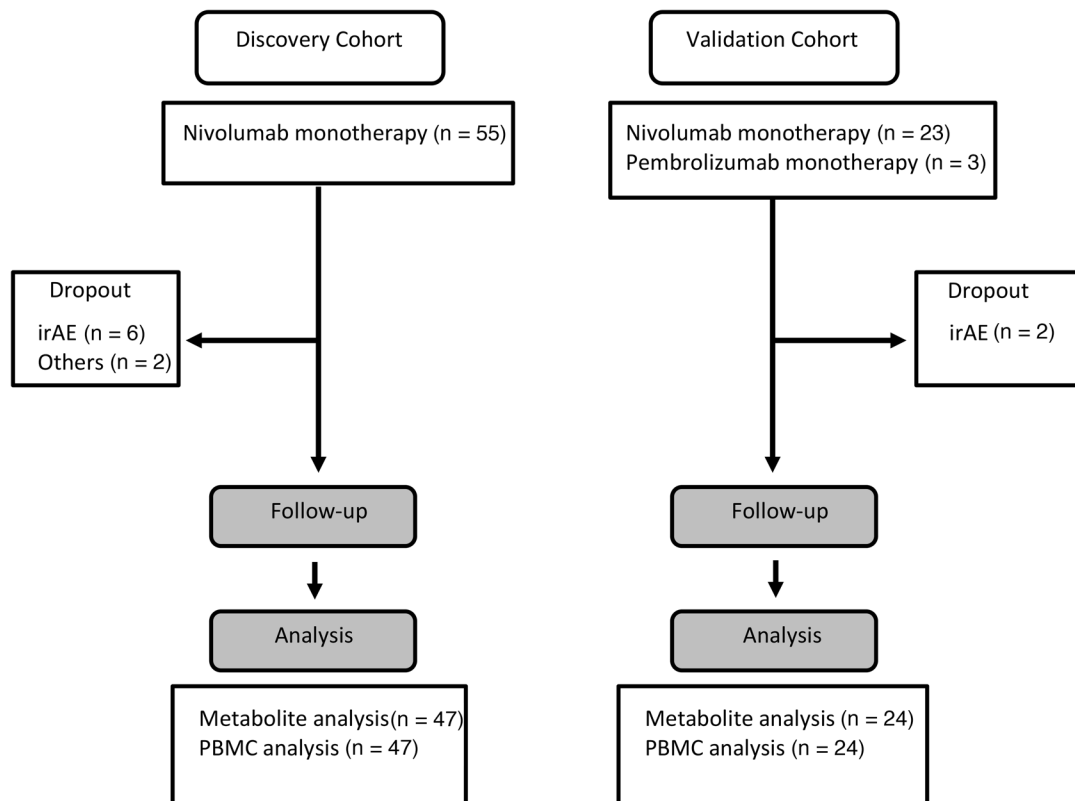
Figure 1. CONSORT flow diagram. irAE, immune-related adverse event.

Therefore, we next used stepwise discriminant analysis to elucidate superior biomarkers based on a combination of metabolites. We first selected those with a significant difference between responders and nonresponders in their levels or in their ratio (fold change) of the different time points among 1482 items in total (247 items × 3 time points + 247 items × 3 ratios) (Supplemental Table 5). A stepwise Akaike's information criterion (AIC) regression procedure against the markers listed in Supplemental Table 5 demonstrated that metabolite combinations I, II, and III were most predictive for the 1st, 1st + 2nd, and 1st + 2nd + 3rd samples, respectively (Table 2 and Supplemental Figure 3). Linear discriminant analysis (LDA) demonstrated that metabolic combination I distinguished between responders and nonresponders with a 23% error rate for 1st samples (Figure 3A). To test the reliability of metabolite combination I, we assigned 47 samples to LDA-R or LDA-NR based on the LDA cutoff value (Figure 3A). As shown in Figure 3B, prediction markers of metabolite combination I could significantly discriminate LDA-R from LDA-NR in PFS. We then found that metabolite combination II distinguished responders and nonresponders with a 22% error rate, and there was a significant difference in both PFS and OS between LDA-R and LDA-NR (Figure 3, C and D). Finally, we found that metabolite combination III discriminated responders and nonresponders with the lowest error rate, 19.6% (Figure 3, E and F). To calculate AUCs of metabolite combinations by discriminant models, we conducted 5-fold cross-validation with logistic regression. In the 5-fold cross-validation, we split the cohort into 5 folds, took the first 20% fold as test data, and trained the prediction model with the remaining 80% to predict into the test data. We iterated this procedure 5 times for each fold and evaluated the model performance with the AUC. As a result, the calculated AUC values were 0.77, 0.83, and 0.91 for the metabolite combinations I, II, and III, respectively, suggesting combination III better discriminated responders and nonresponders (Figure 3G).

Considering that patients are administered nivolumab 6 times over 3 months in the current clinical protocol for NSCLC, metabolite combinations I and II are useful as predictive biomarkers, while metabolite combination III may be less valuable for clinical use despite having the highest reliability.

A combination of cellular markers including mitochondrial activities of CD8^{+} T cells can distinguish between responders and nonresponders. Our previous reports have shown that mitochondrial activation and energy
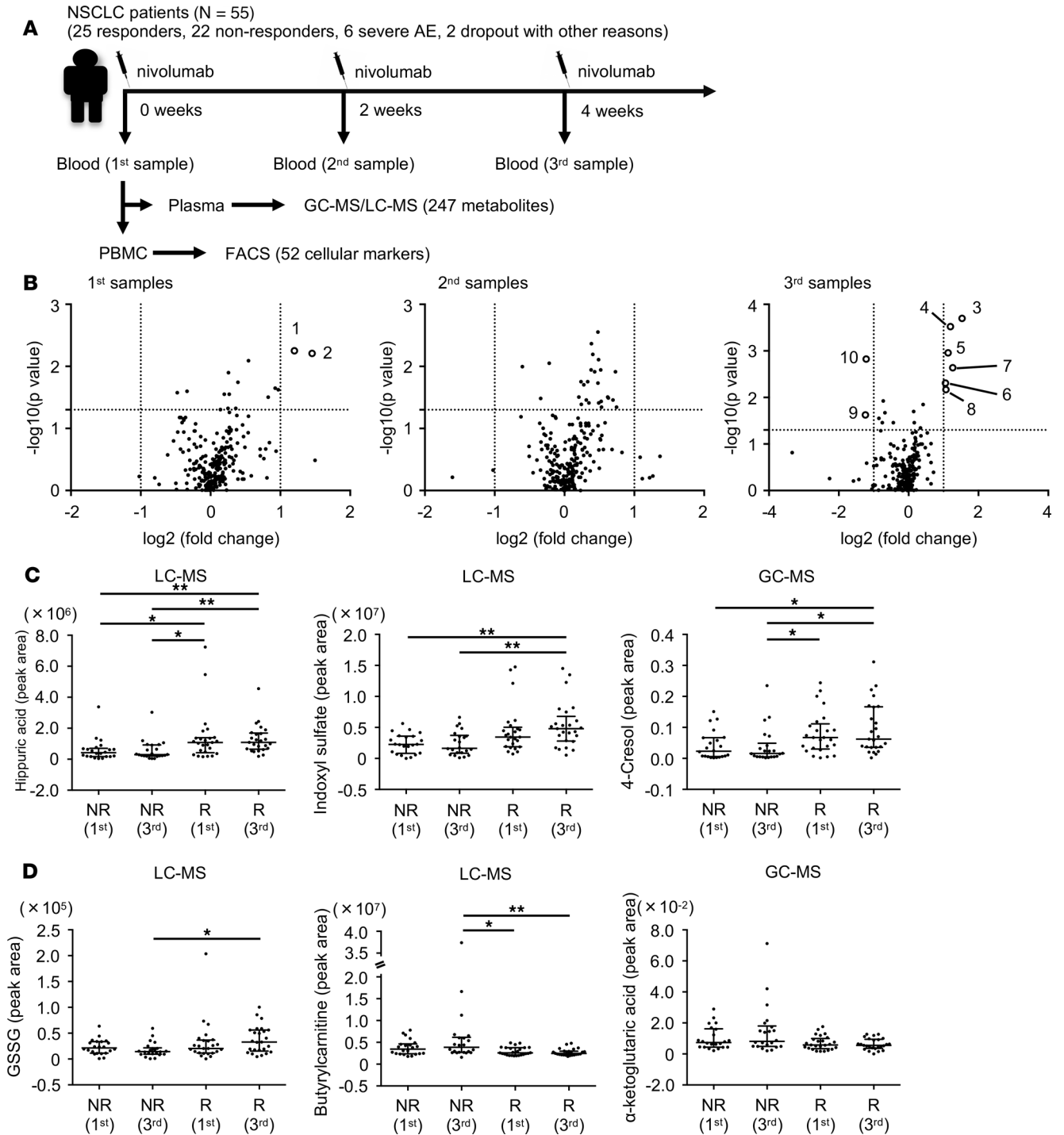
Figure 2. Particular plasma metabolites are associated with nivolumab treatment response. (A) A schematic diagram of this study. GC-MS/LC-MS, gas chromatography–mass spectrometry and liquid chromatography–mass spectrometry. **(B)** Comparison of 247 metabolites between non-responders and responders at each time point was summarized in volcano plots. Metabolites with $\log_2$ |fold change| greater than 1.0 and $-\log_{10}$ (P value) greater than 1.3 were considered significant. Ten metabolites with significant difference between responders and nonresponders are listed in Table 1. **(C)** The peak areas measured by GC-MS or LC-MS of each microbiota-related metabolite in nonresponders (NR) and responders (R). **(D)** The peak areas of redox/energy metabolism–related metabolites. Each dot represents 1 patient. Error bars show median and interquartile range. *$P <$ 0.05; **$P <$ 0.01 by Kruskal-Wallis test followed by Dunn's multiple-comparisons test (**C** and **D**).

metabolism in T cells are strongly associated with the response to the PD-1 blockade therapy (11, 13). Therefore, we simultaneously investigated cellular markers for effector function, energy metabolism, mitochondrial status, and immune activation in CD8+ T cells of the patients' PBMCs. Among the 52 markers shown in Supplemental Table 4 and their ratios between each time point, we found 26 items

Table 1. Ten metabolites with significant difference between responders and nonresponders shown in Figure 2B

Number in Figure 2B	Metabolite name	Timing	Changes in responders relative to nonresponders	Platform[A]	P value[B]	Fold change	AUC[C]
1	Hippuric acid	1st	Higher	LC	0.0056	2.3	0.74
2	Hippuric acid	1st	Higher	GC	0.0062	2.74	0.73
3	Hippuric acid	3rd	Higher	GC	0.0002	2.89	0.81
4	Hippuric acid	3rd	Higher	LC	0.0003	2.3	0.81
5	Indoxyl sulfate	3rd	Higher	LC	0.0011	2.19	0.78
6	Indoxyl sulfate	3rd	Higher	GC	0.0049	2.08	0.74
7	4-Cresol	3rd	Higher	GC	0.0023	2.41	0.76
8	GSSG	3rd	Higher	LC	0.0068	2.1	0.73
9	α-Ketoglutaric acid	3rd	Lower	GC	0.0238	0.42	0.69
10	Butyrylcarnitine	3rd	Lower	LC	0.0015	0.43	0.77

[A]The analytical platform (GC-MS or LC-MS) used for metabolite measurement. [B]P value for distinction between responders and nonresponders (Wilcoxon's rank-sum test). [C]The area under the curve (AUC) of each metabolite in relation to responsiveness was calculated from univariate logistic regression analysis.

with significant differences in the expression levels between responders and nonresponders (Supplemental Table 6). We further selected the best combination of predictive biomarkers from these 26 items using the stepwise method as described for metabolites. As shown in Table 3, the best combinations to predict responders in the 1st, 1st + 2nd, and 1st + 2nd + 3rd samples were designated as cellular marker combinations I, II, and III containing 2, 4, and 4 items, respectively. The marker of responsive patients having a lower PD-1^{hi} population among CD8$^+$ T cells in pretreated samples (in the 1st samples) appeared in all 3 cellular marker combinations, I, II, and III (Figure 4A and Table 3). The cutoff for PD-1^{hi} was defined by the 97th percentile of PD-1 expression intensity (Supplemental Figure 4A). It is important to note that there was no difference between responders and nonresponders in the frequency of total PD-1$^+$CD8$^+$ T cells (Supplemental Figure 4B). Although the PD-1^{hi}CD8$^+$ T cell population appears to vigorously proliferate as the frequency of Ki-67 was higher than PD-1^{lo} or PD-1$^-$CD8$^+$ T cells, it produced less granzyme B and IFN-γ (Supplemental Figure 5). In addition, in PD-1^{hi}CD8$^+$ T cells, T-box expressed in T cells (T-bet) expression was lower, but eomesodermin (EOMES) expression and intensity of Mito SOX were higher than in PD-1^{lo} or PD-1$^-$CD8$^+$ T cells (Supplemental Figure 5). The Ki-67$^+$ T cells increased after treatment (2nd + 3rd) compared with pretreatment (1st) in both PD-1^{hi} and PD-1^{lo} subpopulations, which corresponds to the previous report (Supplemental Figure 5 and ref. 30). The PD-1^{lo} population showed stronger effector phenotypes, such as higher production of granzyme B, IFN-γ, and T-bet, while the PD-1^{hi} population showed lower production of these markers. These data indicate that after PD-1 blockade, highly proliferated T cells express more PD-1 and go into a severe exhaustion state, whereas moderately proliferated T cells express less PD-1 and keep a greater capacity to revive to effector T cells. Indeed, the transcriptional expression array analysis in peripheral CD8$^+$ T cells demonstrated that the frequency of PD-1^{hi} in CD8$^+$ T cells correlated well with the expression levels of *CTLA4* and *TIM3*, known as exhaustion markers (Supplemental Figure 6A). The frequency of subpopulations among PD-1^{hi}CD8$^+$ T cells showed no significant differences between responders and nonresponders, indicating that quantity rather than quality of CD8$^+$PD-1^{hi} T cells was associated with responsiveness (Supplemental Figure 6B). To test the correlation between the PD-1^{hi}CD8$^+$ T cells and tumor antigen load, we also examined the tumor burden as previously described (31). Patients with only nonmeasurable lesions, including 2 responders and 5 nonresponders, were excluded from this analysis of tumor burden. As shown in Supplemental Figure 7A, there was no correlation between PD-1^{hi} frequency and tumor burden. Notably, the tumor burden did not correlate to responsiveness to the PD-1 blockade therapy (Supplemental Figure 7B), suggesting that the tumor burden may not be a determinant of the severity of exhaustion in patients with NSCLC in our study.

Mitochondrial ROS, which is measured by a dye called Mito SOX, is one of the mitochondrial activation indicators (11). We found that the ratio of Mito SOX levels in CD8$^+$ and CD4$^+$ T cells (Mito SOX CD8/CD4) was higher in pretreated responders (1st samples), and this marker was shared by all marker

Table 2. The best predictive combination of metabolites selected by AIC regression procedure

Metabolite combination	Selected metabolite (time point)	Change in responders relative to nonresponders	Samples	Platform	Data in Supplemental Figure 3
I	Cystine (1st)	Higher	1st	GC	A
	Unk8 (1st)	Lower		GC	A
	Hippuric acid (1st)	Higher		LC	A
II	Arabinose (2nd)	Higher	1st + 2nd	GC	B
	Arginine (2nd)	Higher		LC	B
	Butyrylcarnitine (2nd)	Lower		LC	B
III	Hippuric acid (1st)	Higher	1st + 2nd + 3rd	LC	A
	Cystine (2nd)	Higher		GC	C
	GSSG (3rd)	Higher		LC	C
	Butyrylcarnitine (3rd)	Lower		LC	C

combinations as with the PD-1^{hi}CD8$^+$ T cell marker (Table 3 and Figure 4B). These results indicate that higher mitochondrial activation status in CD8$^+$ T cells when normalized by that of CD4$^+$ T cells before treatment is important for a better response (Figure 4B). Because PGC-1 is a master regulator of mitochondrial biogenesis and mitochondrial metabolic pathways, such as oxidative phosphorylation and FAO (32, 33), we addressed PGC-1 expression using a polyclonal antibody that recognizes both PGC-1α and PGC-1β (PGC-1αβ hereafter). Whereas the PGC-1αβ expression in CD8$^+$ T cells decreased in responders between the 1st and 2nd samples, it increased between the 2nd and 3rd samples (Table 3 and Figure 4C). Therefore, the ratio of PGC-1αβ expression in the 2nd relative to 1st samples was lower in responders but higher in the 2nd relative to 3rd samples (Figure 4C). To clarify the mechanism of the quick decline of PGC-1αβ expression following the first nivolumab injection in responders, we investigated the PGC-1αβ expression in each population of CD8$^+$ T cells. As shown in Supplemental Figure 8A, CCR7$^-$CD8$^+$ (effector) T cells have higher PGC-1αβ levels than CCR7$^+$CD8$^+$ (naive) T cells. Importantly, the frequency of CCR7$^-$CD8$^+$ in PBMCs decreased after the first shot of nivolumab in responders (Supplemental Figure 8B). Therefore, the quick decline is presumably because the frequency of CCR7$^-$CD8$^+$ T cells, which have higher PGC-1αβ, decreased in the peripherally circulating PBMCs in responders after nivolumab injection. This interpretation will be discussed later. As other groups have already reported, we also found that the frequency of CD4$^+$ T cells was increased after nivolumab treatment in responders (Table 3, Figure 4D, and ref. 34). Further analysis revealed that nivolumab treatment increased the population of CD4$^+$CD45RO$^+$CCR7$^+$ (central memory) in responders and decreased CD4$^+$CD45RO$^-$CCR7$^-$ (terminally differentiated effector memory CD45RA$^+$ T cells) (Supplemental Figure 9).

A combination of the cellular markers associated with suppressive state and mitochondrial status in T cells is highly predictive. We assessed the error rate of cellular marker combinations I, II, and III by the method described above. LDA demonstrated clear separation between responders and nonresponders with an error rate of 19.1% for cellular combination I (Figure 5A). If we define responders and nonresponders based on the LDA criteria as we did in the metabolic markers, this classification significantly discriminated LDA-R and LDA-NR in both PFS and OS (Figure 5B). The cellular markers in combination I showed higher AUC in a single or combined mode than the PD-L1 TPS usually used in the clinic, indicating the importance of the markers derived from the immune properties of patients rather than those from tumors (Supplemental Table 7, Figure 5B, and Supplemental Figure 1, D and E). LDA of cellular marker combinations II and III predicted both LDA-R and LDA-NR with 4.3% error rates, and there were significant differences ($P < 0.05$) between LDA-R and LDA-NR in both PFS and OS (Figure 5, C–F). AUCs for cellular marker combinations I, II, and III were 0.85, 0.96, and 0.93, respectively, by 5-fold cross-validation with logistic regression within the same cohort (Figure 5G). These data indicate that a combination of cellular biomarkers obtained before the second therapy is sufficient to discriminate between responders and nonresponders. Although it has been reported that patients with EGFR mutations show a different response to the PD-1 blockade therapy (24), those patients could be correctly
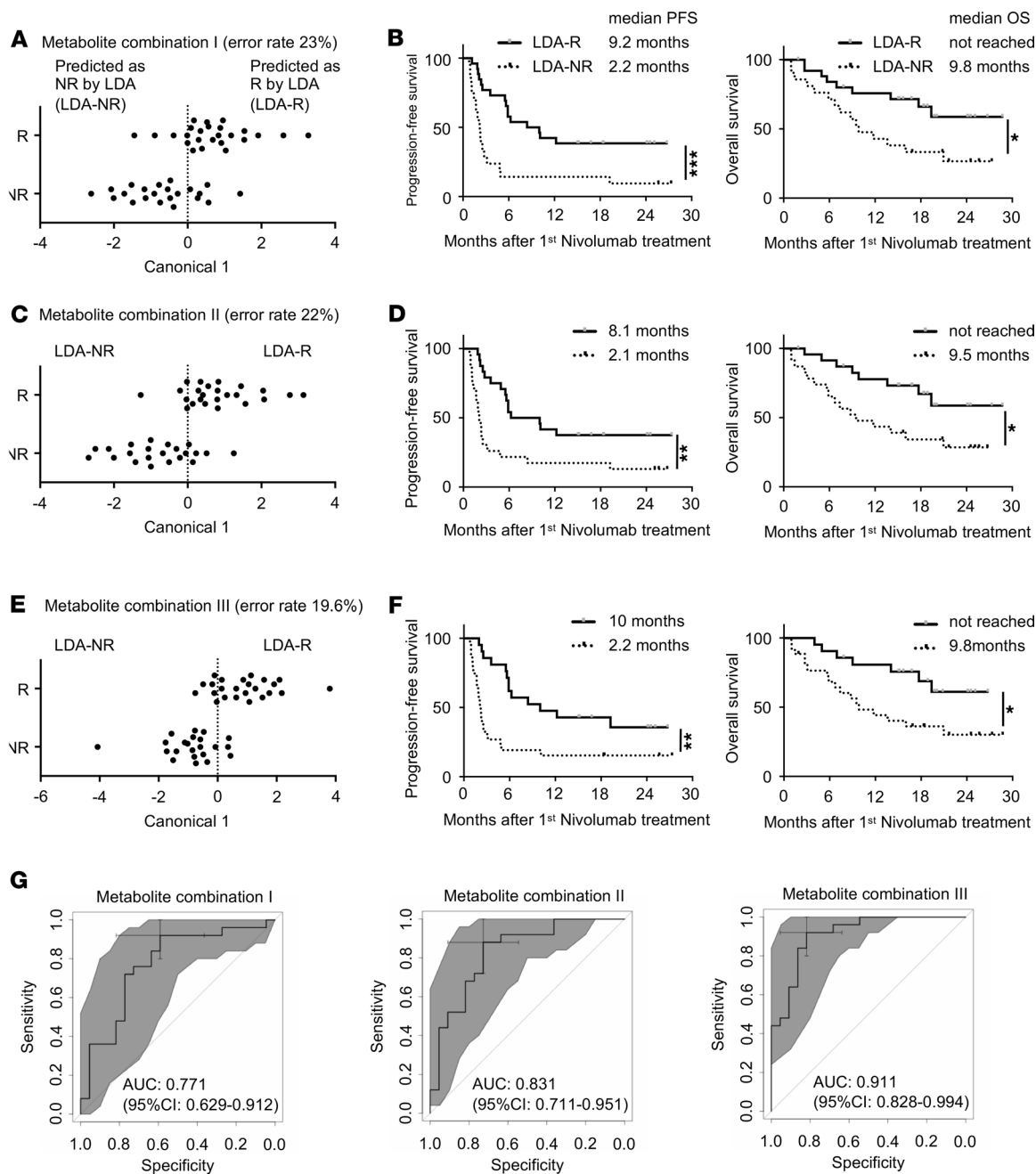
Figure 3. A combination of plasma metabolites predicts responsiveness to nivolumab treatment. (**A**) Linear discriminant analysis (LDA) was used to evaluate the accuracy of metabolite combination I as a predictive biomarker. Canonical plot of LDA for determination of responders (LDA-R) and nonresponders (LDA-NR). Each dot represents 1 patient. The vertical dotted line indicates the cutoff value. (**B**) Kaplan-Meier plots of PFS and OS of LDA-R (solid line) and LDA-NR (dotted line) determined by combination I. (**C**) Canonical plot of LDA based on metabolite combination II. (**D**) Kaplan-Meier plots of PFS and OS of LDA-R and LDA-NR in combination II. (**E**) Canonical plot for LDA based on metabolite combination III. (**F**) Kaplan-Meier plots of PFS and OS of LDA-R and LDA-NR in combination III. *$P < 0.05$; **$P < 0.01$; ***$P < 0.001$ by log-rank test (**B**, **D**, and **F**). (**G**) The ROC curve of 5-fold cross-validation for metabolite combinations I, II, and III.

determined using our cellular marker combination II (Supplemental Figure 10), suggesting that these combination markers based on immune properties may be more useful than tumor property–derived markers alone.

To prospectively validate cellular marker combination II, we measured the 4 cellular markers in a new cohort (validation cohort) of 24 patients (Figure 1). The LDA criteria of cellular marker combination II based on the discovery cohort correctly identified responders and nonresponders with an 8.3 % error rate and AUC was 0.919 with LDA (Figure 5H).

Table 3. The best combination of cellular markers for prediction selected by AIC regression

Cellular marker combination	Selected cellular marker (time point)	Change in responders relative to nonresponders	Samples	Data in Figure 4
I	% of PD-1^{hi} among CD8$^+$ T cells (1st)	Lower	1st	A
	Mito SOX CD8/CD4 (1st)	Higher		B
II	% of PD-1^{hi} among CD8$^+$ T cells (1st)	Lower	1st + 2nd	A
	Mito SOX CD8/CD4 (1st)	Higher		B
	PGC-1αβ of CD8$^+$ T cells (2nd/1st)	Lower		C
	% of CD4$^+$ T cells among PBMCs (2nd/1st)	Higher		D
III	% of PD-1^{hi} among CD8$^+$ T cells (1st)	Lower	1st + 2nd + 3rd	A
	Mito SOX CD8/CD4 (1st)	Higher		B
	PGC-1αβ of CD8$^+$ T cells (3rd/2nd)	Higher		C
	% of CD4$^+$ T cells among PBMCs (2nd/1st)	Higher		D

The metabolic and cellular markers are linked. We next carried out the stepwise method to select the best combination of markers among the total metabolic and cellular markers with significant differences between responders and nonresponders (Supplemental Tables 5 and 6). Surprisingly, all selected markers were derived from cellular markers, resulting in the same combination and results as shown in Table 3. Therefore, we hypothesized that there might be a linkage between responsible metabolic and cellular markers, which might lead us to exclude the metabolic markers. Because cellular combination II was appropriate for prediction and practical for clinical use as described above, we focused on cellular marker combination II and investigated which metabolic markers correlated with each of the cellular markers in the combination. Spearman's correlation coefficients (*r*) were used to measure the association between the cellular and metabolic markers. Generally, |*r*| of more than 0.4 in Spearman's is considered to have a modest to strong correlation. We found that PGC-1αβ expression in CD8$^+$ T cells correlated with the microbiota-related metabolic markers, the frequency of PD-1^{hi}CD8$^+$ T cells correlated with the FAO-related metabolic marker, and the T cell Mito SOX marker was correlated with redox-related metabolic markers (Figure 6A). Note that cystine and pyroglutamic acid are components of glutathione, as shown in Supplemental Figure 11. We further examined the correlation between the frequency of PD-1^{hi}CD8$^+$ T cells and FAO-related gene expression in CD8$^+$ T cells. Importantly, the frequency of PD-1^{hi} (1st) was negatively correlated with the transcriptional expression of carnitine palmitoyltransferase 1B (*CpT1B*) (2nd) (*r* = –0.44), which transports acylcarnitine from the cytoplasm into the mitochondria (27–29), suggesting the reduced function of acylcarnitine transportation in PD-1^{hi} T cells (Supplemental Figure 12). Corresponding to this mechanism, in these patients, the frequency of PD-1^{hi} population also correlated with butyrylcarnitine 3rd/1st and hexanoylcarnitine 2nd/1st (Figure 6A and Supplemental Figure 12), demonstrating that the frequency of the PD-1^{hi} marker correlated with plasma increases in these acylcarnitine families after nivolumab treatment. This interpretation will be discussed later.

Cluster analysis showed a relative correlation weight between cellular combination II and metabolic markers, which can be classified into the 3 groups of (a) microbiota-related metabolites, (b) FAO-related metabolites, and (c) redox-related metabolites (Figure 6B). Details of the correlation between cellular markers and metabolite markers are summarized in Table 4. In conclusion, stepwise discriminant analysis among all markers excluded the responsible metabolic markers because they were closely linked with particular cellular markers that had slightly more predictive value than the metabolic markers. The current data support a link between microbiota activity and T cell energy metabolism, both of which contribute to the power of antitumor immunity and responsiveness to the PD-1 blockade immunotherapy.
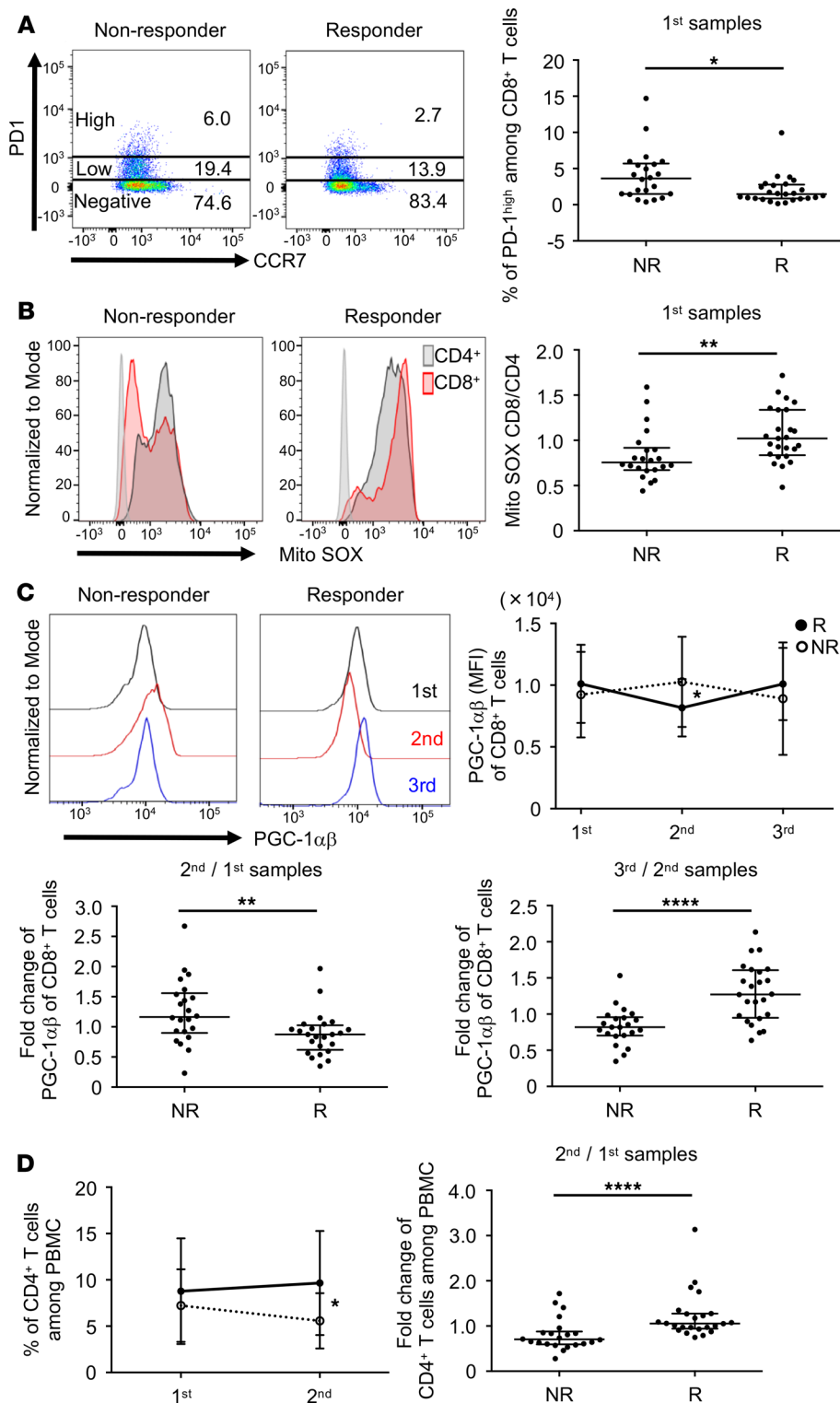
Figure 4. Particular cellular markers, including mitochondria status, were selected to make up a combinatorial predictive marker. (**A**) Two representative NSCLC samples (nonresponder and responder) showing PD-1 and CCR7 positivity after gating on CD8+ PBMCs (left). Frequency of PD-1hiCD8+ T cells in nonresponders and responders in the 1st samples (right). (**B**) Representative histograms of Mito SOX on gated CD4+ (black) and CD8+ (red) T cells (left). Ratio of Mito SOX levels in CD8+ and CD4+ T cells (Mito SOX CD8/CD4) for nonresponders and responders in the 1st samples (right). (**C**) PGC-1αβ of the 1st (black), 2nd (red), and 3rd (blue) samples among CD8+ PBMCs (upper left). MFI of PGC-1αβ between the 1st, 2nd, and 3rd samples (upper right). The solid line and dotted line represent responders and nonresponders, respectively. Fold change of PGC-1αβ expression between nonresponders and responders in the 2nd relative to 1st samples (lower left) and the 3rd relative to 2nd samples (lower right). (**D**) Frequency of CD4+ T cells among PBMCs in the 1st and 2nd samples (left). The solid line and dotted line represent responders and nonresponders, respectively. Fold change of CD4+ T cell frequency in the 2nd relative to 1st samples between nonresponders and responders (right). Each dot represents 1 patient. Error bars show median and interquartile range. *$P < 0.05$; **$P < 0.01$; ****$P < 0.0001$ by Wilcoxon's rank-sum test.

Discussion

In this study, we first demonstrated that the combination of several cellular markers of T cell activation status, including T cell mitochondrial condition, could effectively discriminate responders from nonresponders. The correlation analysis revealed that the functional activity of CD8+ T cells was related to a complex network of different higher-order function systems, such as the microbiome and energy metabolism. The advantages of our findings are summarized as follows: (a) we showed that each AUC of our immune property–based markers is higher than that of the hitherto clinically approved biomarker, PD-L1 TPS; (b) blood-based tests to examine
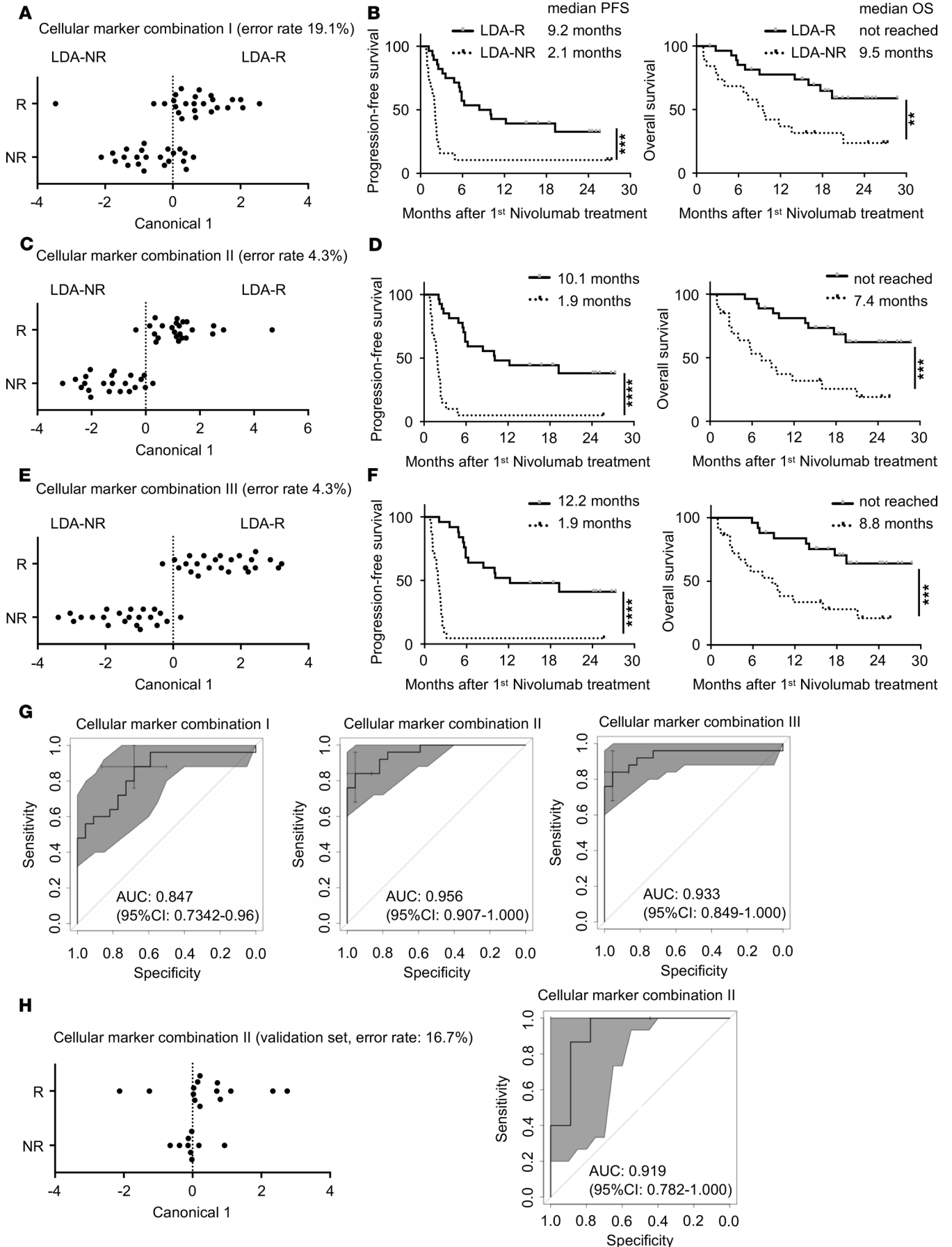
Figure 5. A combination of cellular markers could predict survival more precisely. (**A**) LDA evaluated accuracy of cellular marker combination I. Canonical plot of LDA for determination of LDA-R and LDA-NR. Each dot represents 1 patient. The vertical dotted line indicates the cutoff value. (**B**) Kaplan-Meier plots of PFS and OS of LDA-R (solid line) and LDA-NR (dotted line) on cellular marker combination I. (**C**) Canonical plot for LDA based on cellular marker combination II. (**D**) Kaplan-Meier plots of PFS and OS of LDA-R and LDA-NR on cellular marker combination II. (**E**) Canonical plot for LDA based on cellular marker combination III. (**F**) Kaplan-Meier plots of PFS and OS of LDA-R and LDA-NR on cellular marker combination III. **$P < 0.01$; ***$P < 0.001$; ****$P < 0.0001$ by log-rank test (**B**, **D**, and **F**). (**G**) The ROC curve of 5-fold cross-validation for cellular marker combinations I, II, and III. (**H**) Canonical plot and ROC curve for prospective validation cohort with LDA based on cellular marker combination II.

immune cell properties and/or metabolites would be much simpler and more patient-friendly because testing phenotypes of tumors usually puts a huge burden on patients; and (c) combination of immune property–based biomarkers is more powerful than several single immune property–based biomarkers so far proposed (16).

One of the microbiota-derived metabolites, hippuric acid, which was higher in the pretreated samples of responders, could be an indicator of microbiome diversity and is produced preferentially by *Clostridiales* (35, 36). Diversity of microbiota and the ratio of *Clostridiales* are reported to be higher in PD-1 blockade therapy responders, which supports our results that hippuric acid is higher in responders. So far, identification of particular strains of microbiota involved in antitumor activation is still quite difficult because of numerous species of microbiota in the gut (17). However, measuring a few common metabolites, such as hippuric acid, indoxyl sulfate, and 4-cresol, produced by numerous kinds of microbiota would facilitate the quick, comprehensive evaluation of microbiota status without deep sequencing of microbiota 16s rRNA. Considering that the levels of microbiota-derived metabolites correlated with PGC-1αβ expression levels in CD8+ T cells, some components of microbiota may affect the mitochondrial activation of peripheral CD8+ T cells, though the mechanism behind microbiota regulation of peripheral CD8+ T cells remains largely unknown (18).

We showed that the temporal reduction of PGC-1αβ may be due to the decrement of effector CD8+ T cells (CCR7– population) from the blood, which express higher PGC-1αβ than CD8+ naive T cells (CCR7+ population). We and other groups previously indicated the cancer-immunity cycle theory is critical for robust antitumor immunity where effector T cells traffic to the tumor site, guided by the gradient of IFN-γ–induced chemokines released from the tumor site during the PD-1 blockade therapy (8, 11). Therefore, it is anticipated that PD-1 blockade triggers the trafficking of peripheral effector T cells to the tumor site preferentially in the responders. Given that microbiota affect the activation status of effector T cells (17, 35, 36), it would be reasonable that plasma hippuric acid levels and PGC-1αβ expression in the peripheral CD8+ T cells have moderate to high correlation with each other because PGC-1αβ expression is higher in effector CD8+ T cells than naive CD8+ T cells.

We previously reported that FAO is important to produce sufficient ATP, which is required for longevity in effector T cells (13). When FAO is promoted, acylcarnitines are substantially transported into the mitochondrial matrix, resulting in the reduction of acylcarnitine levels in the plasma (27–29, 37, 38). Therefore, plasma levels of acylcarnitine species could be an indicator of robustness in mitochondrial function or FAO usage in inflammation mediated by immunity (39–41). In the present study, acylcarnitines (butyrylcarnitine, isovalerylcarnitine, and hexanoylcarnitine) were elevated in nonresponders, especially in the latter seconnd and third phases, suggesting that the function of FAO in CD8+ T cells is attenuated in nonresponders (38). The substantial correlation between higher acylcarnitine levels and higher frequency of PD-1hiCD8+ T cells suggests the presence of a large number of severely exhausted CD8+ T cells, which have a weaker FAO function in nonresponders. Indeed, the frequency of PD-1hi negatively correlated with the transcriptional expression of *CpT1B* in CD8+ T cells, which serves as a transporter of acylcarnitine families from cytoplasm into mitochondria. Given that (a) PD-1loCD8+ T cells proliferated less and retained the effector function and (b) PD-1loCD8+ T cells had lower levels of CTLA-4 and Tim-3 based on correlation analysis, it is likely that PD-1hiCD8+ T cells are in irreversible exhaustion states associated with the FAO defect in the periphery. However, the precise mechanistic linkage of FAO defect and T cell dysfunction is largely unknown.

Although we recruited 55 and 26 patients for the discovery and validation cohorts, respectively, the cohorts are rather small to obtain high reliability. However, validation is difficult in a larger cohort under the same conditions because the use of PD-1 blockade antibody single therapy is currently very rare because of the clinical strategy of combination therapy in patients with NSCLC. It will be important to test our biomarkers for the combination therapy as well in the future. Considering the convenience of specific metabolite measurement and the difficulties in technical variations for cellular marker measurements between different facilities, the combination of particular metabolites might be more practical in the clinic. Our new insight sheds light on the use of combinatorial biomarkers for cancer immunotherapy, which would provide nonresponders another opportunity to have immunotherapy and improve therapeutic efficacy.
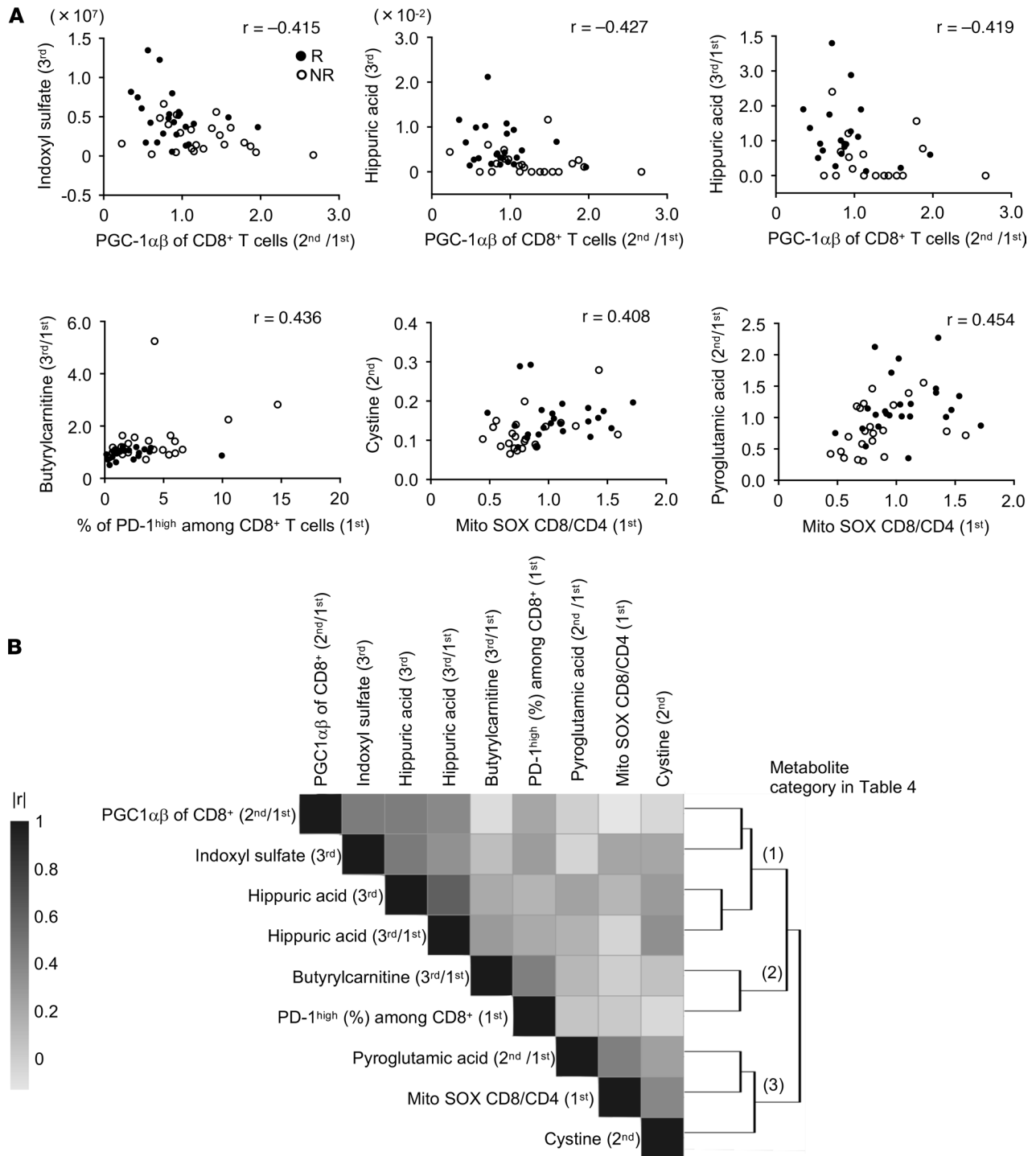
Figure 6. Modest correlation between particular cellular and metabolite markers excludes metabolite makers from the combinatorial candidate biomarker. (A) Scatter plots between cellular markers (*x* axis) and metabolite markers (*y* axis). The dots represent the responders and the circles indicate the nonresponders. *r*, Spearman's correlation coefficients. Generally, |*r*| of more than 0.4 in Spearman's is considered to have a modest to strong correlation. **(B)** A clustered heatmap of absolute correlation coefficients over all marker pairs detected in **A** (using Spearman's correlation distance and complete linkage). Dark denotes higher correlation (|*r*| close to 1) and light lower correlation (|*r*| close to 0). The markers clustered into 3 groups, which were designated as metabolic categories I, II, and III.

Methods

Study design and participants. The study subjects, patients with NSCLC receiving nivolumab (anti–PD-1 blocking antibody) at Kyoto University Hospital, consented to the collection and storage of blood samples during treatment and allowed review of their medical records for past medical history, cancer tumor

Table 4. Correlation between cellular and metabolite markers

Cellular markers (Change in responders relative to nonresponders)	Metabolite markers (Change in responders relative to nonresponders)	Metabolite category
PGC-1αβ of CD8⁺ T cells (2nd/1st) (lower)	Indoxyl sulfate (3rd) (higher)	(I) Microbiome-related metabolites
	Hippuric acid (3rd) (higher)	
	Hippuric acid (3rd/1st) (higher)	
Percentage of PD-1ʰⁱ among CD8⁺ T cells (1st) (lower)	Butyrylcarnitine (3rd/1st) (lower)	(II) FAO-related metabolites
Mito SOX CD8/CD4 (1st) (higher)	Cystine (2nd) (higher)	(III) Redox-related metabolites
	Pyroglutamic acid (2nd/1st) (higher)	

type, toxicity assessments, and clinical response, survival, and laboratory data. We enrolled 55 patients with NSCLC, all of whom had previously received other chemotherapy. This study included 39 male and 16 female patients, aged between 31 and 83 years (median 68). Forty-three patients (78.2% among all patients) were diagnosed with adenocarcinoma, including 9 patients with EGFR mutation (17.3% among 52 patients) and 3 patients with anaplastic lymphoma kinase translocation (6.8% among 44 patients) (Supplemental Table 1). Patients received nivolumab (3 mg/kg) through i.v. infusion every 2 weeks (1 cycle) until disease progression or the emergence of an unacceptable side effect. At a median follow-up time of 455 days (range, 29 to 861 days), the median PFS and OS were 147 days (95% CI, 76 to 300 days) and 629 days (95% CI, 408 days to not reached), respectively (Supplemental Figure 1A). Among 55 patients enrolled, 8 patients had to stop the therapy because of severe side effects and other reasons (Figure 1). Blood samples were collected just before the first, second, and third nivolumab injection. Tumor size was measured by CT and evaluated for response using Response Evaluation Criteria in Solid Tumors 1.1. Total measurable tumor burden was defined as the sum of the long axis of all measurable lesions of the pretreatment CT as previously described (31). To assess PD-L1 expression, we performed PD-L1 IHC using the PD-L1 IHC 22C3 pharmDx kit (Agilent Technologies) as previously described (42). TPS was defined as tumor PD-L1 expression frequency. PD-L1 TPS was classified into PD-L1 negative, weakly positive, or strongly positive (<1%, 1%–49 %, and ≥50%, respectively) (42).

For the prospective validation study, 26 patients with NSCLC who had received nivolumab or pembrolizumab at Kyoto University Hospital were independently enrolled. Of these 26, 2 had to stop the therapy because of severe side effects, leaving us with the data of 24 patients for analysis (Figure 1). For functional analysis of the PD-1ʰⁱCD8⁺ T cell population, we assessed 16 patients among 24 patients enrolled for the validation.

Thirty healthy blood donors were recruited at the Medical Examination Center at Takeda Hospital. Their age was between 46 and 78 (mean 66) years, and they included 22 male and 8 female donors.

Sample preparation for plasma metabolome measurement. Peripheral blood samples were collected in 7-mL EDTA vacutainers (Venoject II, VP-NA070K), immediately stored in a CubeCooler (Forte Grow Medical Co. Ltd.), and kept at 4°C until centrifugation at 4°C at 1800 g for 15 minutes. All the harvested plasma samples were then stored at −80°C until analysis. For GC-MS analysis, 50 μL of plasma was mixed with 256 μL of a solvent mixture (methanol/water/chloroform = 2.5:1:1) containing 2.34 μg/mL of 2-isopropylmalic acid (MilliporeSigma), which was used as an internal standard. The obtained mixture was shaken at 1200 rpm for 30 minutes at 37°C (Maximizer MBR-022UP, Taitec). After centrifugation at 16,000 g for 5 minutes at 25°C, 150 μL of supernatant was collected and mixed with 140 μL of purified water followed by vortex mixing for 5 seconds. After centrifugation at 16,000 g for 5 minutes at 25°C, 180 μL of supernatant was dried in a centrifugal evaporator (CVE-3100, Tokyo Rikakikai Co. Ltd.). The dried sample was dissolved in 80 μL of methoxyamine solution (20 mg/mL in pyridine, MilliporeSigma) and shaken at 1200 rpm for 30 minutes at 37°C. Forty microliters of *N*-methyl-*N*-trimethylsilyl-trifluoroacetamide solution (GL Sciences) was added for trimethylsilyl derivatization, followed by agitation at 1200 rpm for 30 minutes at 37°C. After centrifugation, 50 μL of supernatant was transferred to a glass vial and subjected to GC-MS measurement. For LC-MS analysis, the metabolite extraction protocol was slightly changed. Fifty microli-

ters of plasma was mixed with 256 μL of methanol and shaken at 1200 rpm for 10 minutes at 37°C. After centrifugation at 16,000 g for 30 minutes at 25°C, 150 μL of supernatant was mixed with 90 μL of 1% acetic acid in water and 120 μL of chloroform, followed by vortex mixing for 15 seconds. After centrifugation at 2000 g for 10 minutes at 25°C, 150 μL of the upper layer was dried and solubilized in 50 μL of 0.1% formic acid in water and then subjected to LC-MS analysis.

Plasma metabolome analysis. GC-MS analysis was performed with a GCMS-QP2010 Ultra (Shimadzu). The derivatized metabolites were separated on a DB-5 column (30 m × 0.25 mm inner diameter, film thickness 1.0 μm, Agilent Technologies). The helium carrier gas was set at a flow rate of 39 cm/s. The inlet temperature was 280°C and the column temperature was first held at 80°C for 2 minutes, then raised at a rate of 15°C/min to 330°C and held for 6 minutes. One microliter of the sample was injected into the GC-MS in the split mode (split ratio 1:3). The mass spectra were obtained under the following conditions: electron ionization (ionization voltage 70 eV), ion source temperature 200°C, interface temperature 250°C, and full scan mode in the range of m/z 85 to 500 and scan rate 0.3 s/scan. Identification of chromatographic peaks was performed using the National Institute of Standards and Technology Research Library or Shimadzu GC/MS database and further confirmed with authentic commercial standards. For semiquantitative analysis, the area of each metabolite peak was calculated and divided by the area of the internal standard peak. LC separation was conducted on a Shim-pack GIST C18-AQ column (3 μm, 150 mm × 2.1 mm id, Shimadzu GLC) with a Nexera UHPLC system (Shimadzu). The mobile phase consisted of 0.1% formic acid in water (A) and 0.1% formic acid in acetonitrile (B). The gradient program was as follows: 0 to 3 minutes, 0% B; 3 to 15 minutes, linear gradient to 60% B; 15.0 to 17.5 minutes, 95% B; 17.5 to 20.0 minutes, linear gradient to 0% B; hold for 4 minutes; flow rate, 0.2 mL/min. The column oven temperature was maintained at 40°C. The LC system was coupled with a triple-quadrupole mass spectrometer, LCMS-8060 (Shimadzu). LCMS-8060 was operated with the electrospray ionization and multiple reaction monitoring mode. All ion transitions and collision energies were optimized experimentally by using authentic standards of each metabolite. Three microliters of the sample was injected into the LC-MS system. Quality control (QC, pooled plasma) samples were subjected to the same preparation protocol and injected every 10 and 5 samples for GC-MS and LC-MS analysis, respectively. Each metabolite's signals were normalized with a QC-based correction method using the smooth-spline algorithm (43–45). Information on all the measured metabolites, including retention time, m/z, and ion transitions, is summarized in Supplemental Tables 2 and 3.

Flow cytometry. Fresh PBMCs were isolated by Ficoll density gradient centrifugation. PBMCs were immediately stained using the following antibodies: anti-CD8a (RPA-T8, TONBO), -CD8 (SK1, TONBO), -CD4 (RPA-T4, SK3, TONBO), -CD45RA (HI100, TONBO), -CD45RO (UCHL1, BioLegend), -CCR7 (3D12, eBioscience), –PD-1 (EH12.2H7, BioLegend), -Tim3 (F38-2E2, BioLegend), -KLRG1 (13F12F2, eBioscience), -CD25 (BC96, BioLegend), -CXCR3 (G025H7, BioLegend), -CCR6 (G034E3, BioLegend), –T-bet (4B10, BioLegend), -EOMES (WD1928, eBioscience), –Ki-67 (SolA15, eBioscience), –CTLA-4 (BNI3, TONBO), –p-mTOR (MRRBY, eBioscience), –p-Akt1 (Ser473) (SDRNR, eBioscience), –granzyme B (GB11, BioLegend), –IFN-γ (4S.B3, BD Biosciences), and -FOXP3 (236A/E7, BD Biosciences). PGC-1 expression was detected by anti–PGC-1αβ (rabbit polyclonal, Abcam, ab72230), which recognizes both PGC-1α and PGC-1β, followed by secondary staining with goat anti-rabbit IgG (Santa Cruz Biotechnology, sc-3739). Live/dead cell discrimination was performed using 7-AAD staining solution (TONBO, 13-6993). Intracellular staining was performed using a FOXP3 fixation kit (eBioscience). For assessment of intracellular phosphoproteins, cells were permeabilized with 0.5% Triton X-100 and fixed with 1.5% paraformaldehyde before staining. Acquisition of samples was carried out on the BD FACSCanto II cell analyzer (BD Biosciences). Data were collected using the BD FACSDiva Software version 6.1.3 and further analyzed with FlowJo 10.4 (Tree Star Inc.). Data were gated on live (7-AAD⁻) and single cells. Determination of mitochondrial mass, membrane potential, mitochondrial superoxide, and cellular ROS was performed using MitoTracker Green, MitoTracker Deep Red, MitoSOX Red, and CellROX Green reagents, respectively (all from Life Technologies). These dyes were added to cells and incubated at 37°C in a 5% CO_2 humidified incubator for 30 minutes, followed by surface staining. Intracellular staining for granzyme B and IFN-γ was performed following treatment with plate-bound anti-CD3 (OKT3, TONBO) and anti-CD28 (55725, BD Pharmingen) for 6 hours in the presence of Brefeldin A (eBioscience) and Monensin (eBioscience) for the last 4 hours. After nivolumab treatment, anti–PD-1 (EH12.2H7, APC conjugated, BioLegend) antibody was added to cells and incubated at 37°C in a 5% CO_2 humidified incubator for 60 minutes, followed by other surface staining.

Microarray analysis of patients' CD8⁺ T cells. We isolated peripheral CD8⁺ T cells from the same cohorts available (1st samples, $n = 33$; 2nd samples, $n = 27$). CD8⁺ T cells were purified from patients' PBMCs by AutoMACS according to the manufacturer's instructions (Miltenyi Biotec, 130-045-201).

Total RNA was isolated with RNeasy Micro Kit (Qiagen). The quality of extracted RNA was analyzed using TapeStation (Agilent Technologies). Five nanograms of total RNA was labeled using the GeneChip WT Pico Reagent Kit (Thermo Fisher Scientific) and hybridized to GeneChip Clariom D Assay, Human (Thermo Fisher Scientific). The array data were analyzed using Signal Space Transformation-Robust Multi-Chip Analysis and Sketch-Quantile normalization (Expression Console Software). Then we applied the Linear Models for Microarray Analysis (limma) package of Bioconductor software (46) and obtained differentially expressed genes. Functional analysis of the decreased gene expression was performed using the Database for Annotation, Visualization and Integrated Discovery (http://david.ncifcrf.gov) (47). Microarray data have been deposited under Gene Expression Omnibus accession number GSE141479.

Statistics. Data are reported as the median and interquartile range. A Wilcoxon rank-sum test was conducted to compare the 2 groups. A Kruskal-Wallis test followed by Dunn's test for multiple comparisons were conducted to compare the difference across independent groups. The stepwise AIC regression procedure was performed to select the best marker combination. Then LDA was performed by using the estimated biomarker combination to predict the reliability and failure rate. To adjust the cutoff value to 0, we changed the constant value of the equation of LDA as shown in Supplemental Table 8. For the validation study, we used the same equation as LDA combination II. The prediction model was evaluated with 5-fold cross-validation and LDA to calculate AUCs for the discovery and validation cohorts, respectively. The survival rates of different groups of patients were calculated with the Kaplan-Meier method and presented graphically as a survival curve. A comparison of survival curves between 2 groups was tested by log-rank test. Spearman's or Pearson's correlation coefficient was used to calculate the association between the cellular markers, the metabolic markers, and gene expression levels. JMP software (version 12.0.0; SAS Institute Inc.), R software (version 3.4.4), DataRobot (version 4.3.0), and Prism software (version 6.0h; GraphPad Software) were used for data management and statistical analyses. Significance levels were set at $P < 0.05$ for all tests.

Study approval. All patient and donor samples were obtained from subjects who provided informed consent for blood use in accordance with the Declaration of Helsinki and with approval from the Ethics Committee of Kyoto University (G1012).

Author contributions

RH, KC, KS, SK, MA, FM, and T. Honjo analyzed and interpreted data. RH, KC, YHK, HY, HO, YS, IM, and T. Hirai collected clinical samples and analyzed clinical data. RH, KT, SK, YO, and FM performed statistical analysis. KC, SF, and T. Honjo supervised the study. RH, KC, KS, KT, SK, and T. Honjo prepared the manuscript. YHK, SF, YO, FM, IM, and T. Hirai critically reviewed the manuscript.

Acknowledgments

Address correspondence to: Tasuku Honjo, Department of Immunology and Genomic Medicine, Kyoto University Graduate School of Medicine, Yoshida Konoe-cho, Sakyo-ku, Kyoto, 606-8501, Japan. Phone: 81.75.753.4371; Email: honjo@mfour.med.kyoto-u.ac.jp.

1. Dunn GP, Old LJ, Schreiber RD. The immunobiology of cancer immunosurveillance and immunoediting. *Immunity*. 2004;21(2):137–148.
2. Leach DR, Krummel MF, Allison JP. Enhancement of antitumor immunity by CTLA-4 blockade. *Science*. 1996;271(5256):1734–1736.
3. Iwai Y, Ishida M, Tanaka Y, Okazaki T, Honjo T, Minato N. Involvement of PD-L1 on tumor cells in the escape from host

immune system and tumor immunotherapy by PD-L1 blockade. *Proc Natl Acad Sci USA*. 2002;99(19):12293–12297.

4. Iwai Y, Hamanishi J, Chamoto K, Honjo T. Cancer immunotherapies targeting the PD-1 signaling pathway. *J Biomed Sci*. 2017;24(1):26.

5. Hodi FS, et al. Improved survival with ipilimumab in patients with metastatic melanoma. *N Engl J Med*. 2010;363(8):711–723.

6. Topalian SL, et al. Safety, activity, and immune correlates of anti-PD-1 antibody in cancer. *N Engl J Med*. 2012;366(26):2443–2454.

7. McLane LM, Abdel-Hakeem MS, Wherry EJ. CD8 T cell exhaustion during chronic viral infection and cancer. *Annu Rev Immunol*. 2019;37:457–495.

8. Chen DS, Mellman I. Oncology meets immunology: the cancer-immunity cycle. *Immunity*. 2013;39(1):1–10.

9. Buck MD, O'Sullivan D, Pearce EL. T cell metabolism drives immunity. *J Exp Med*. 2015;212(9):1345–1360.

10. Miyajima M, et al. Metabolic shift induced by systemic activation of T cells in PD-1-deficient mice perturbs brain monoamines and emotional behavior. *Nat Immunol*. 2017;18(12):1342–1352.

11. Chamoto K, et al. Mitochondrial activation chemicals synergize with surface receptor PD-1 blockade for T cell-dependent antitumor activity. *Proc Natl Acad Sci USA*. 2017;114(5):E761–E770.

12. Murphy MP, Siegel RM. Mitochondrial ROS fire up T cell activation. *Immunity*. 2013;38(2):201–202.

13. Chowdhury PS, Chamoto K, Kumar A, Honjo T. PPAR-induced fatty acid oxidation in t cells increases the number of tumor-reactive CD8+ T cells and facilitates anti-PD-1 therapy. *Cancer Immunol Res*. 2018;6(11):1375–1387.

14. Fagarasan S, Muramatsu M, Suzuki K, Nagaoka H, Hiai H, Honjo T. Critical roles of activation-induced cytidine deaminase in the homeostasis of gut flora. *Science*. 2002;298(5597):1424–1427.

15. Kawamoto S, et al. The inhibitory receptor PD-1 regulates IgA selection and bacterial composition in the gut. *Science*. 2012;336(6080):485–489.

16. Mitsuhashi A, Okuma Y. Perspective on immune oncology with liquid biopsy, peripheral blood mononuclear cells, and microbiome with non-invasive biomarkers in cancer patients. *Clin Transl Oncol*. 2018;20(8):966–974.

17. Gopalakrishnan V, et al. Gut microbiome modulates response to anti-PD-1 immunotherapy in melanoma patients. *Science*. 2018;359(6371):97–103.

18. Routy B, et al. Gut microbiome influences efficacy of PD-1-based immunotherapy against epithelial tumors. *Science*. 2018;359(6371):91–97.

19. Topalian SL, Drake CG, Pardoll DM. Immune checkpoint blockade: a common denominator approach to cancer therapy. *Cancer Cell*. 2015;27(4):450–461.

20. Zou W, Wolchok JD, Chen L. PD-L1 (B7-H1) and PD-1 pathway blockade for cancer therapy: mechanisms, response biomarkers, and combinations. *Sci Transl Med*. 2016;8(328):328rv4.

21. Le DT, et al. Mismatch repair deficiency predicts response of solid tumors to PD-1 blockade. *Science*. 2017;357(6349):409–413.

22. Geltink RIK, Kyle RL, Pearce EL. Unraveling the complex interplay between T cell metabolism and function. *Annu Rev Immunol*. 2018;36:461–488.

23. Brahmer J, et al. Nivolumab versus docetaxel in advanced squamous-cell non-small-cell lung cancer. *N Engl J Med*. 2015;373(2):123–135.

24. Borghaei H, et al. Nivolumab versus docetaxel in advanced nonsquamous non-small-cell lung cancer. *N Engl J Med*. 2015;373(17):1627–1639.

25. Wikoff WR, et al. Metabolomics analysis reveals large effects of gut microflora on mammalian blood metabolites. *Proc Natl Acad Sci USA*. 2009;106(10):3698–3703.

26. Franchina DG, He F, Brenner D. Survival of the fittest: Cancer challenges T cell metabolism. *Cancer Lett*. 2018;412:216–223.

27. Jones LL, McDonald DA, Borum PR. Acylcarnitines: role in brain. *Prog Lipid Res*. 2010;49(1):61–75.

28. Schooneman MG, Vaz FM, Houten SM, Soeters MR. Acylcarnitines: reflecting or inflicting insulin resistance? *Diabetes*. 2013;62(1):1–8.

29. Rinaldo P, Cowan TM, Matern D. Acylcarnitine profile analysis. *Genet Med*. 2008;10(2):151–156.

30. Kamphorst AO, et al. Proliferation of PD-1+ CD8 T cells in peripheral blood after PD-1-targeted therapy in lung cancer patients. *Proc Natl Acad Sci USA*. 2017;114(19):4993–4998.

31. Huang AC, et al. T-cell invigoration to tumour burden ratio associated with anti-PD-1 response. *Nature*. 2017;545(7652):60–65.

32. Ventura-Clapier R, Garnier A, Veksler V. Transcriptional control of mitochondrial biogenesis: the central role of PGC-1alpha. *Cardiovasc Res*. 2008;79(2):208–217.

33. Scharping NE, et al. The tumor microenvironment represses T cell mitochondrial biogenesis to drive intratumoral T cell metabolic insufficiency and dysfunction. *Immunity*. 2016;45(2):374–388.

34. Takeuchi Y, Tanemura A, Tada Y, Katayama I, Kumanogoh A, Nishikawa H. Clinical response to PD-1 blockade correlates with a sub-fraction of peripheral central memory CD4+ T cells in patients with malignant melanoma. *Int Immunol*. 2018;30(1):13–22.

35. Pallister T, et al. Hippurate as a metabolomic marker of gut microbiome diversity: Modulation by diet and relationship to metabolic syndrome. *Sci Rep*. 2017;7(1):13670.

36. Li M, et al. Symbiotic gut microbes modulate human metabolic phenotypes. *Proc Natl Acad Sci USA*. 2008;105(6):2117–2122.

37. Koves TR, et al. Mitochondrial overload and incomplete fatty acid oxidation contribute to skeletal muscle insulin resistance. *Cell Metab*. 2008;7(1):45–56.

38. Gatza E, et al. Manipulating the bioenergetics of alloreactive T cells causes their selective apoptosis and arrests graft-versus-host disease. *Sci Transl Med*. 2011;3(67):67ra8.

39. Mihalik SJ, et al. Increased levels of plasma acylcarnitines in obesity and type 2 diabetes and identification of a marker of glucolipotoxicity. *Obesity (Silver Spring)*. 2010;18(9):1695–1700.

40. Sun L, et al. Early prediction of developing type 2 diabetes by plasma acylcarnitines: a population-based study. *Diabetes Care*. 2016;39(9):1563–1570.

41. Ruiz M, et al. Circulating acylcarnitine profile in human heart failure: a surrogate of fatty acid metabolic dysregulation in mitochondria and beyond. *Am J Physiol Heart Circ Physiol*. 2017;313(4):H768–H781.

42. Yasuda Y, Ozasa H, Kim YH. PD-L1 Expression in small cell lung cancer. *J Thorac Oncol*. 2018;13(3):e40–e41.

43. Dunn WB, et al. Procedures for large-scale metabolic profiling of serum and plasma using gas chromatography and liquid chromatography coupled to mass spectrometry. *Nat Protoc*. 2011;6(7):1060–1083.

44. Kirwan JA, Broadhurst DI, Davidson RL, Viant MR. Characterising and correcting batch variation in an automated direct infusion mass spectrometry (DIMS) metabolomics workflow. *Anal Bioanal Chem*. 2013;405(15):5147–5157.

45. Rusilowicz M, Dickinson M, Charlton A, O'Keefe S, Wilson J. A batch correction method for liquid chromatography-mass spectrometry data that does not depend on quality control samples. *Metabolomics*. 2016;12:56.

46. Gentleman RC, et al. Bioconductor: open software development for computational biology and bioinformatics. *Genome Biol*. 2004;5(10):R80.

47. Huang da W, Sherman BT, Lempicki RA. Systematic and integrative analysis of large gene lists using DAVID bioinformatics resources. *Nat Protoc*. 2009;4(1):44–57.